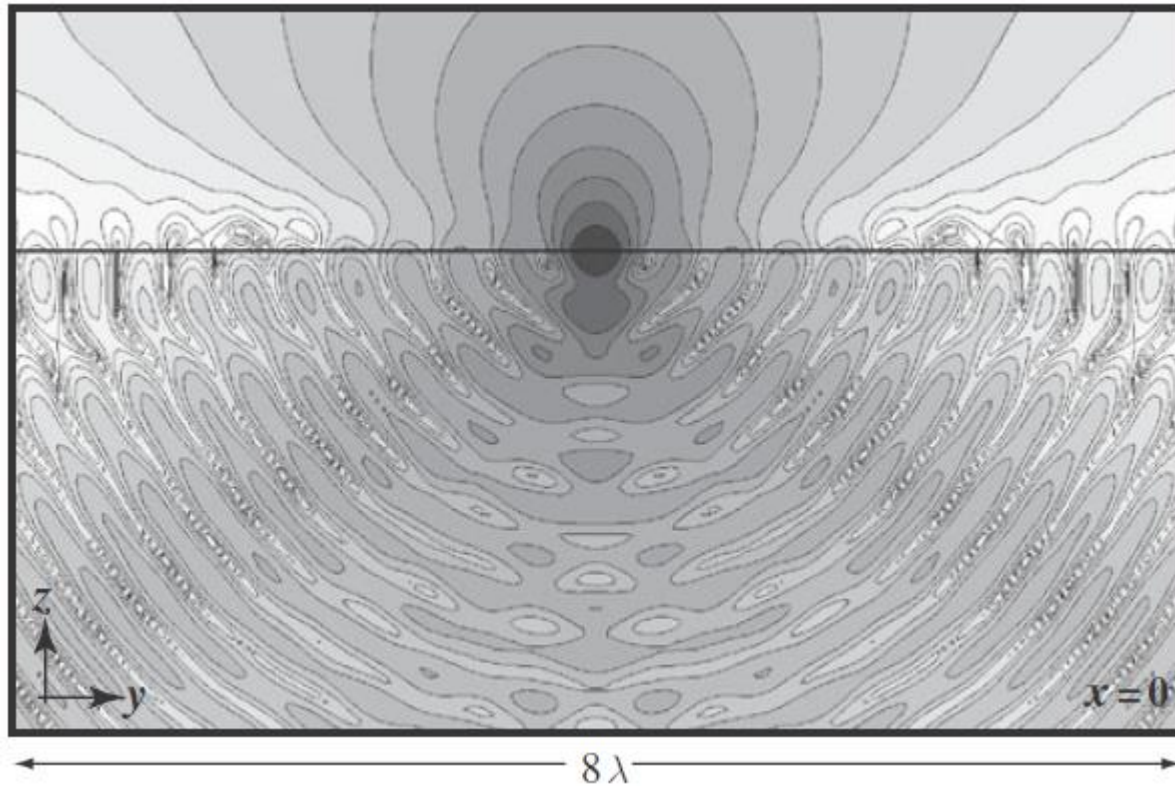
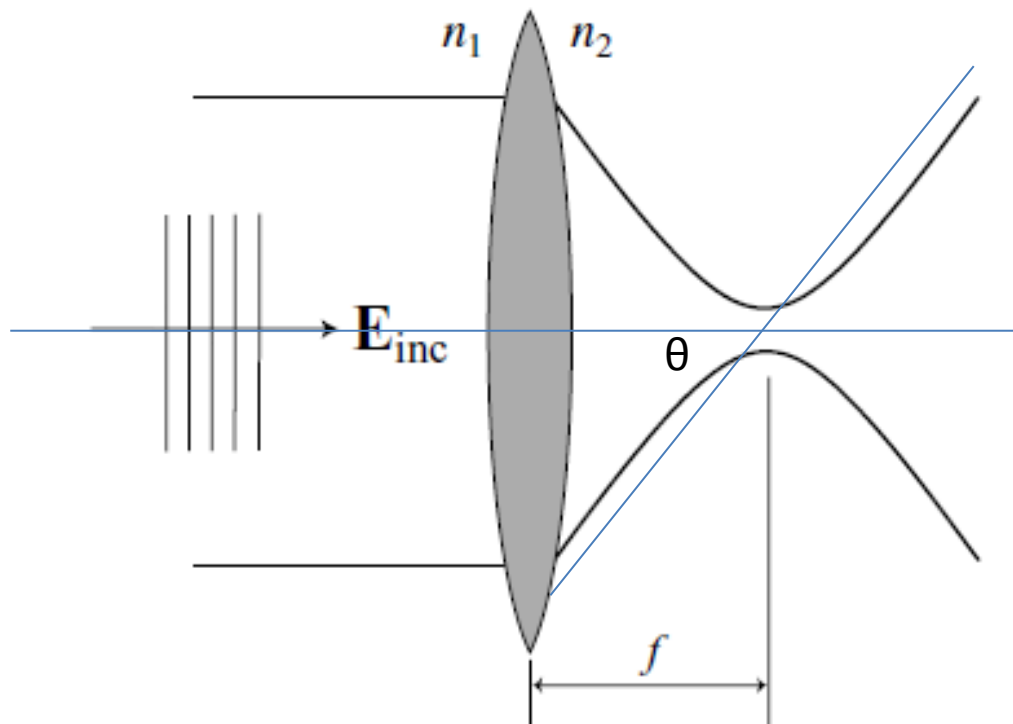


strongly focused beam



Strongly focused beam

The paraxial approximation is no longer valid when the numerical aperture of the system is close to 1



$$NA = n \sin \theta$$

Figure 3.5 Focusing of a laser beam by an aplanatic lens.

Aspherical lenses have a much smaller focus spot than spherical lenses

Spherical Lenses



Achromatic Lenses



Aspheric Lenses

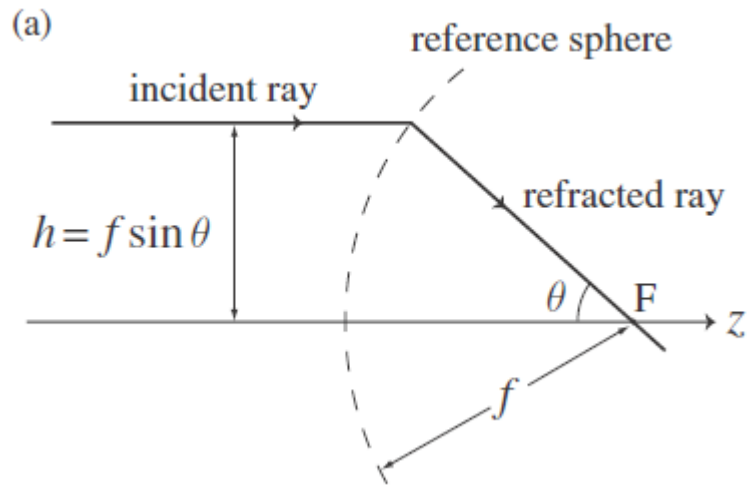


Spherical lens: only good in the paraxial condition ☹ , dispersion ☹

Achromatic lens: only good in the paraxial condition ☹ , no dispersion ☺

Aspherical lens: excellent for all the angles ☺, dispersion ☹

Calculation of strongly focused beam



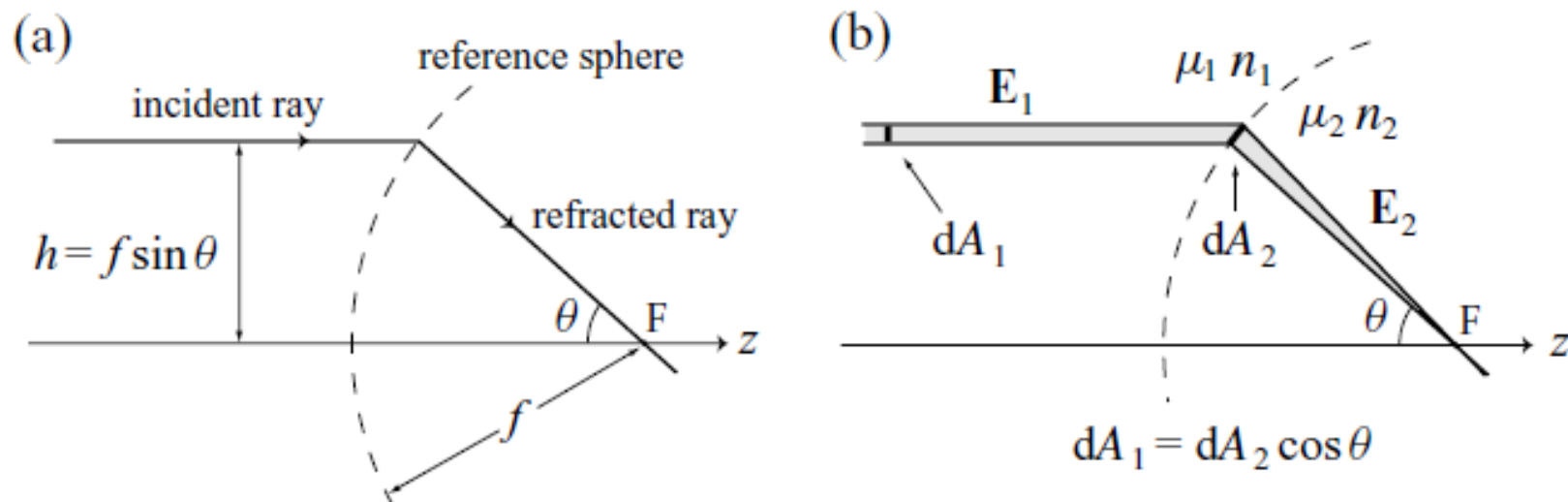


Figure 3.6 (a) Sine condition of Geometrical Optics. The refraction of light rays at an aplanatic lens is determined by a spherical surface with radius f . (b) Intensity law of Geometrical Optics. The energy carried along a ray must stay constant.

power transported by a ray is $dP = (1/2)Z_{\mu\epsilon}^{-1} |\mathbf{E}|^2 dA$, where $Z_{\mu\epsilon}$ is the wave impedance and dA is an infinitesimal cross-section perpendicular to the ray propagation. Thus, as indicated in Fig. 3.7(b), the fields before and after refraction must satisfy

$$|\mathbf{E}_2| = |\mathbf{E}_1| \sqrt{\frac{n_1}{n_2}} \sqrt{\frac{\mu_2}{\mu_1}} (\cos \theta)^{1/2}.$$

Before the lens:

$$\mathbf{E}_{\text{inc}}^{(s)} = [\mathbf{E}_{\text{inc}} \cdot \mathbf{n}_\phi] \mathbf{n}_\phi,$$

$$\mathbf{E}_{\text{inc}}^{(p)} = [\mathbf{E}_{\text{inc}} \cdot \mathbf{n}_\rho] \mathbf{n}_\rho.$$

After the lens:

$$\mathbf{E}_\infty = \left[t^s [\mathbf{E}_{\text{inc}} \cdot \mathbf{n}_\phi] \mathbf{n}_\phi + t^p [\mathbf{E}_{\text{inc}} \cdot \mathbf{n}_\rho] \mathbf{n}_\theta \right] \sqrt{\frac{n_1}{n_2}} (\cos \theta)^{1/2}.$$

Here, t_s , t_p is the transmittance for the s, and p polarization, respectively.

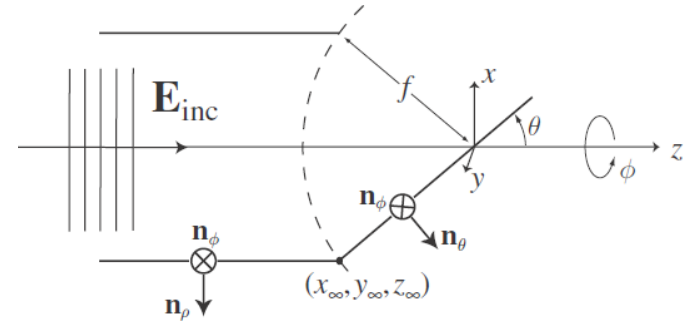
$\sqrt{\frac{n_1}{n_2}} (\cos \theta)^{1/2}$ Comes from the intensity change by the reflection

Transformation between coordinates

$$\mathbf{n}_\rho = \cos \phi \mathbf{n}_x + \sin \phi \mathbf{n}_y,$$

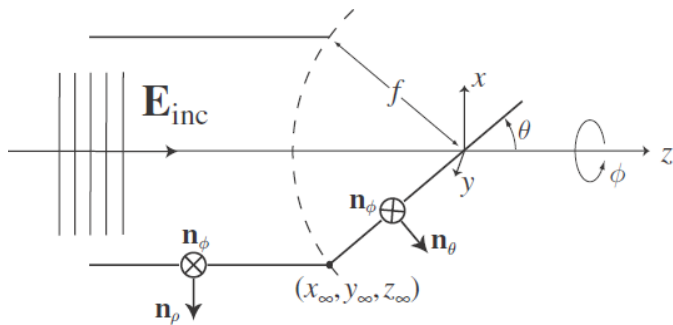
$$\mathbf{n}_\phi = -\sin \phi \mathbf{n}_x + \cos \phi \mathbf{n}_y,$$

$$\mathbf{n}_\theta = \cos \theta \cos \phi \mathbf{n}_x + \cos \theta \sin \phi \mathbf{n}_y - \sin \theta \mathbf{n}_z.$$

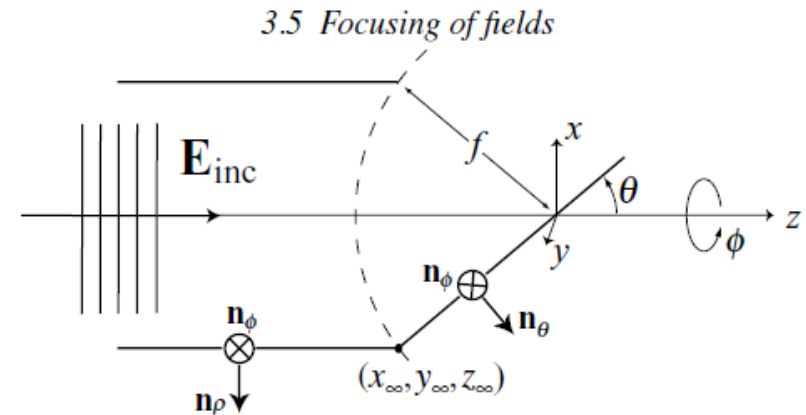
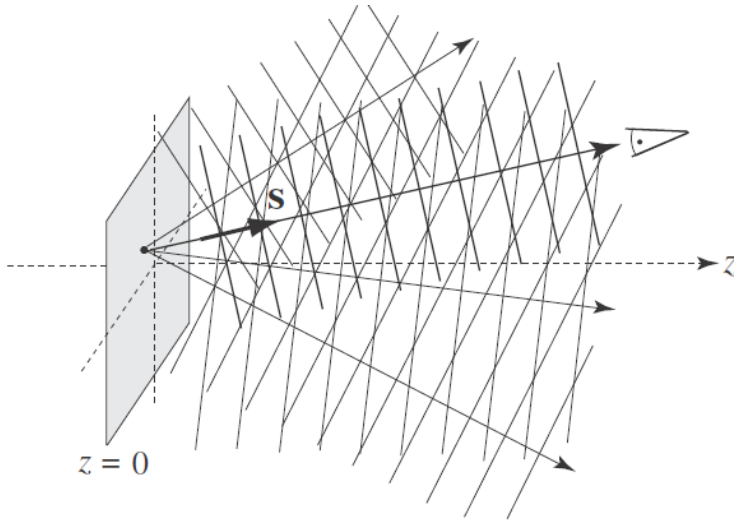


$$\mathbf{E}_{\infty} = \left[t^s [\mathbf{E}_{\text{inc}} \cdot \mathbf{n}_{\phi}] \mathbf{n}_{\phi} + t^p [\mathbf{E}_{\text{inc}} \cdot \mathbf{n}_{\rho}] \mathbf{n}_{\theta} \right] \sqrt{\frac{n_1}{n_2}} (\cos \theta)^{1/2}.$$

$$\begin{aligned} \mathbf{E}_{\infty}(\theta, \phi) = & t^s(\theta) \left[\mathbf{E}_{\text{inc}}(\theta, \phi) \cdot \begin{pmatrix} -\sin \phi \\ \cos \phi \\ 0 \end{pmatrix} \right] \begin{pmatrix} -\sin \phi \\ \cos \phi \\ 0 \end{pmatrix} \sqrt{\frac{n_1}{n_2}} (\cos \theta)^{1/2} \\ & + t^p(\theta) \left[\mathbf{E}_{\text{inc}}(\theta, \phi) \cdot \begin{pmatrix} \cos \phi \\ \sin \phi \\ 0 \end{pmatrix} \right] \begin{pmatrix} \cos \phi \cos \theta \\ \sin \phi \cos \theta \\ -\sin \theta \end{pmatrix} \sqrt{\frac{n_1}{n_2}} (\cos \theta)^{1/2}, \end{aligned}$$



Focusing – from rectangular system to spherical system



$$E(x, y, z) = \frac{ire^{-ikr}}{2\pi} \iint_{(k_x^2 + k_y^2) \leq k^2} E_\infty \left(\frac{k_x}{k}, \frac{k_y}{k} \right) e^{i[k_x x + k_y y \pm k_z z]} \frac{1}{k_z} dk_x dk_y.$$

$$x = \rho \cos \varphi, \quad y = \rho \sin \varphi.$$

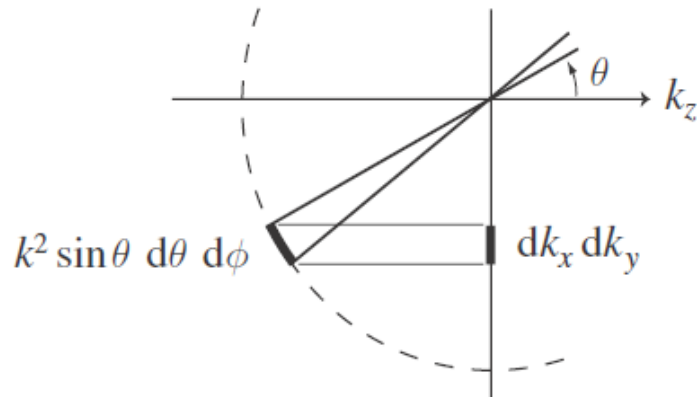
$$k_x = k \sin \theta \cos \phi, \quad k_y = k \sin \theta \sin \phi, \quad k_z = k \cos \theta.$$

$$\frac{1}{k_z} dk_x dk_y = k \sin \theta d\theta d\phi,$$

$$E(\rho, \varphi, z) = -\frac{ikfe^{-ikf}}{2\pi} \int_0^{\theta_{\max}} \int_0^{2\pi} E_\infty(\theta, \phi) e^{ikz \cos \theta} e^{ik\rho \sin \theta \cos(\phi - \varphi)} \sin \theta d\phi d\theta.$$

Focusing – Fourier Optics

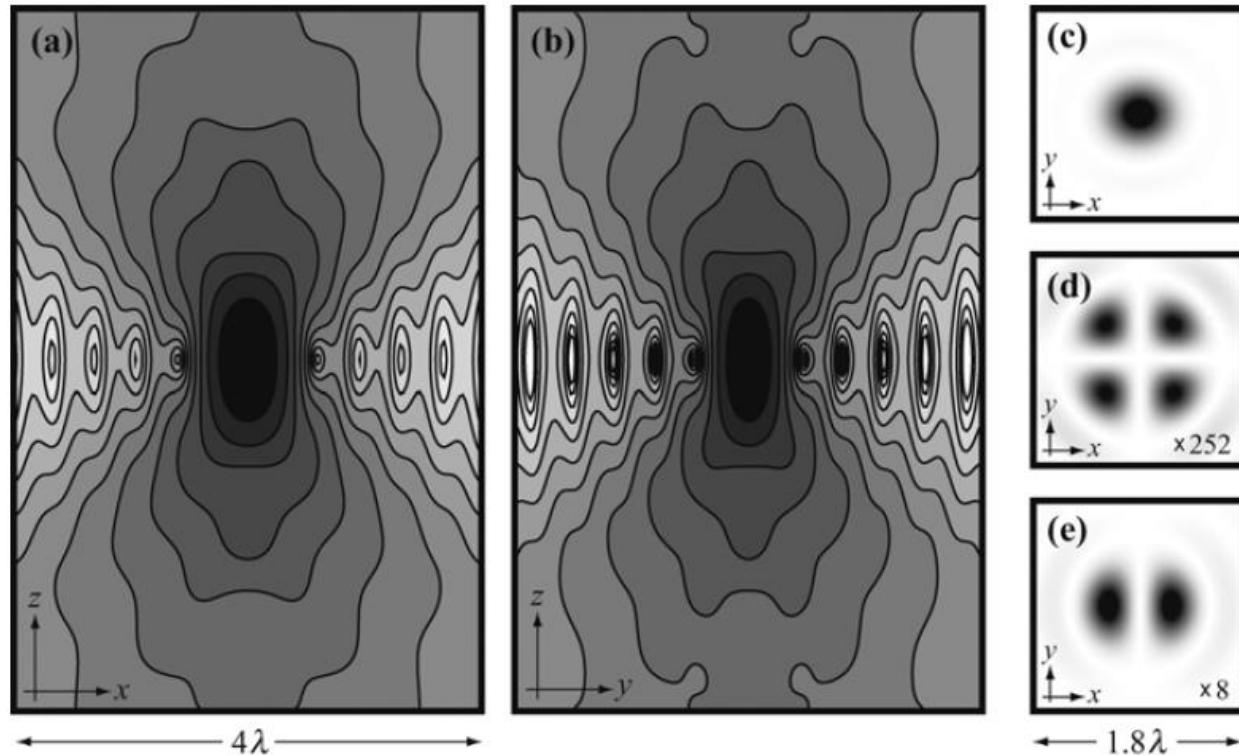
$$\text{NA} = n \sin \theta_{\max} \quad (0 < \theta_{\max} < \pi/2),$$



$$\mathbf{E}(\rho, \varphi, z) = -\frac{ikf e^{-ikf}}{2\pi} \int_0^{\theta_{\max}} \int_0^{2\pi} \mathbf{E}_{\infty}(\theta, \phi) e^{ikz \cos \theta} e^{ik\rho \sin \theta \cos(\phi - \varphi)} \sin \theta d\phi d\theta.$$

In practice, NA decides the limit of angle in the integral

Strongly focused Gaussian beam



Contour plots of constant $|\mathbf{E}|^2$ in the focal region of a focused Gaussian beam ($\text{NA} = 1.4$, $n = 1.518$, $f_0 = 1$): (a) in the plane of incident polarization (x, z); (b) in the plane perpendicular to the plane of incident polarization (y, z). A logarithmic scaling is used, with a factor of 2 difference between adjacent contour lines. Images (c), (d), and (e) show the magnitudes of the individual field components $|E_x|^2$, $|E_y|^2$, and $|E_z|^2$, respectively, in the focal plane ($z=0$).

Focused high order modes

Linearly polarized doughnut mode:

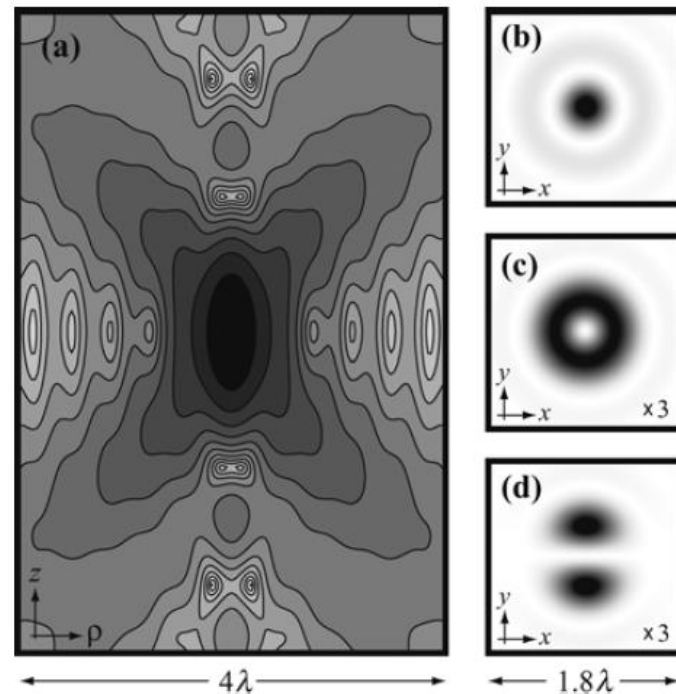
$$LP = HG_{10} \mathbf{n}_x + i HG_{01} \mathbf{n}_y$$

Radially polarized doughnut mode:

$$RP = HG_{10} \mathbf{n}_x + HG_{01} \mathbf{n}_y$$

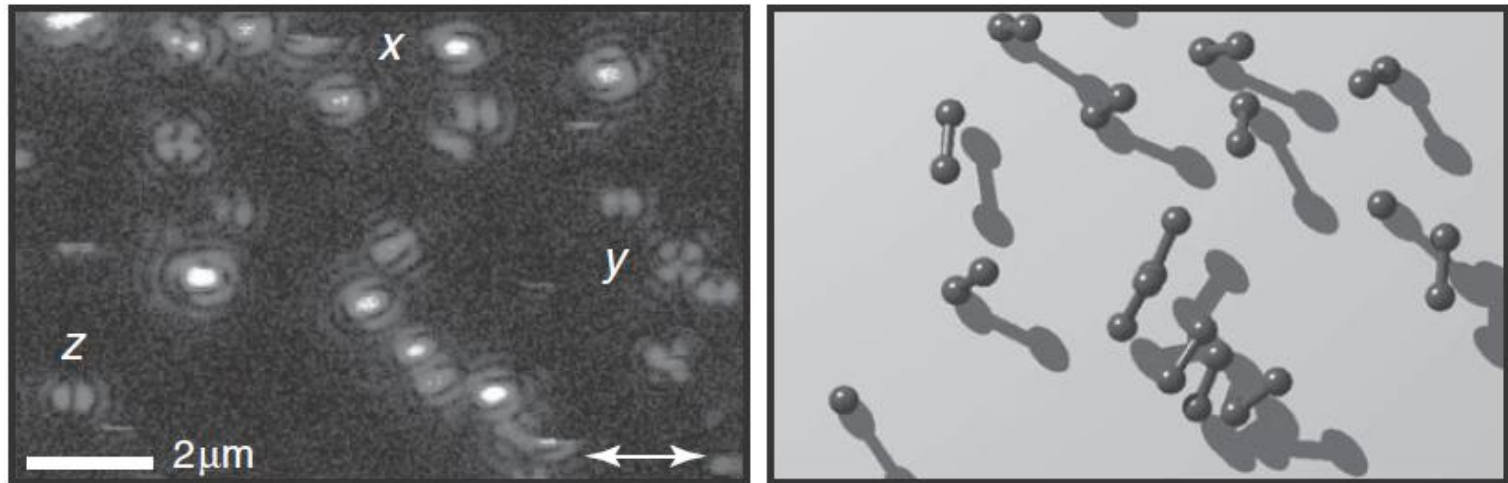
Azimuthally polarized doughnut mode:

$$AP = -HG_{01} \mathbf{n}_x + HG_{10} \mathbf{n}_y.$$



(a) Contour plots of constant $|\mathbf{E}|^2$ in the focal region of a focused radially polarized doughnut mode ($NA = 1.4$, $n = 1.518$, $f_0 = 1$) in the (ρ, z) plane. The intensity is rotationally symmetric with respect to the z -axis. A logarithmic scaling is used with a factor of 2 difference between adjacent contour lines. Images (b), (c), and (d) show the magnitudes of the individual field components $|\mathbf{E}_z|^2$, $|\mathbf{E}_\rho|^2$, and $|\mathbf{E}_y|^2$, respectively, in the focal plane ($z = 0$). A linear scale is used.

Mapping focus spot using single molecule fluorescence imaging



Single-molecule excitation patterns. A sample with isolated single molecules is raster scanned in the focal plane of a strongly focused laser beam. For each pixel, the fluorescence intensity is recorded and encoded in the color scale. The excitation rate in each pixel is determined by the relative orientation of the local electric field vector and the molecular absorption dipole moment. Using the known field distribution in the laser focus allows the dipole moments to be reconstructed from the recorded patterns. Compare the patterns marked x , y , and z with those in Fig. 3.11.